Nano Res. 2011, 4(9): 870–881
DOI 10.1007/s12274-011-0143-8
Research Article

ISSN 1998-0124
CN 11-5974/O4

Binder-Free Activated Carbon/Carbon Nanotube Paper Electrodes for Use in Supercapacitors

Guanghui Xu[1], Chao Zheng[1], Qiang Zhang[1], Jiaqi Huang[1], Mengqiang Zhao[1], Jingqi Nie[1], Xianghua Wang[2], and Fei Wei[1] (✉)

[1] Beijing Key Laboratory of Green Chemical Reaction Engineering and Technology, Department of Chemical Engineering, Tsinghua University, Beijing 100084, China
[2] CNGC Wuzhou Engineering Design and Research Institute, Beijing 100053, China

Received: 23 March 2011 / Revised: 22 April 2011 / Accepted: 25 April 2011

ABSTRACT

Novel inexpensive, light, flexible, and even rollup or wearable devices are required for multi-functional portable electronics and developing new versatile and flexible electrode materials as alternatives to the materials used in contemporary batteries and supercapacitors is a key challenge. Here, binder-free activated carbon (AC)/carbon nanotube (CNT) paper electrodes for use in advanced supercapacitors have been fabricated based on low-cost, industrial-grade aligned CNTs. By a two-step shearing strategy, aligned CNTs were dispersed into individual long CNTs, and then 90 wt%–99 wt% of AC powder was incorporated into the CNT pulp and the AC/CNT paper electrode was fabricated by deposition on a filter. The specific capacity, rate performance, and power density of the AC/CNT paper electrode were better than the corresponding values for an AC/acetylene black electrode. The capacity reached a maximum value of 267.6 F/g with a CNT loading of 5 wt%, and the energy density and power density were 22.5 W·h/kg and 7.3 kW/kg at a high current density of 20 A/g. The AC/CNT paper electrode also showed a good cycle performance, with 97.5% of the original capacity retained after 5000 cycles at a scan rate of 200 mV/s. This method affords not only a promising paper-like nanocomposite for use in low-cost and flexible supercapacitors, but also a general way of fabricating multi-functional paper-like CNT-based nanocomposites for use in devices such as flexible lithium ion batteries and solar cells.

KEYWORDS

Supercapacitor, flexible, energy storage, carbon nanotube, activated carbon

1. Introduction

Portable electronic devices (such as mobile phones, notebooks, and cameras) are becoming more and more multi-functional. Novel inexpensive, light, flexible and even rollup or wearable electronic devices are required [1–4]. Thus, it is necessary to develop new versatile and flexible electrode materials as alternatives to the materials used in contemporary energy conversion and storage devices such as batteries and supercapacitors [3–10].

Among various advanced functional materials, electronically conducting polymers (such as polypyrrole (PPy) and polyaniline (PANI)) and metal oxides (such as RuO_2, MnO_2, NiO, and Co_3O_4) [11–16] are widely used in supercapacitors. However, their applications

Address correspondence to wf-dce@tsinghua.edu.cn

are severely limited by their poor solubility and mechanical brittleness [11]. Anchoring the conductive polymers or metal oxides to cellulose fibers or other textile fibers has inspired the design of their paper- or textile-based composites which show excellent cycling stability, mechanical flexibility and robustness [4, 11, 17]. However, the textile fibers are usually insulators. Advanced carbon materials, such as carbon nanotubes (CNTs) [18–21], graphene [14, 20, 22, 23], ordered mesoporous carbon [24–26], carbon aerogels [13, 26], hierarchical porous carbon [27], carbide-derived carbon [28], and their composites/hybrids [29–35], have been widely explored for use as supercapacitor electrodes. The carbon materials can also be combined with conductive polymers or metal oxides to obtain flexible CNT/PANI [36, 37], carbon nanofiber (CNF)/PANI [10], graphene/PANI or graphene oxide/PANI [14, 16, 38], or CNT/CuO [39] composite electrodes with improved electrochemical performance. Very recently, biscrolling nanotube sheets and functional guests into yarns, which contained up to 95 wt% of otherwise unspinnable particulate or nanofiber powders, has been used to fabricate yarns for use in supercapacitors and lithium-ion battery materials [40]. However, the large scale production of inexpensive, flexible electrode remains a great challenge.

Activated carbon (AC), which is widely used in commercial products, is a cheap electrode material with a high surface area giving a moderate capacity in supercapacitors [31]. It can be divided into AC particles or powder and AC fiber cloth. The AC in powder form is difficult to handle as an electrode material. Thus, conductive agents (carbon black) and binder (poly(tetrafluoroethylene) (PTFE)) are always needed. Recently, CNTs, which can be mass produced by fluidized bed chemical vapor deposition (CVD) at low cost, have been used as conductive agents and/or the electrochemical active phase for advanced electrodes. Supercapacitors with AC/CNT nanocomposite electrodes have been shown to exhibit enhanced electrochemical performance compared with CNT-free carbon materials [30, 41–44], although the original CNTs were strongly entangled with each other, and acid purification was always required. As a result, those CNTs well-dispersed in the electrode were too short to form a self-supporting network. The as-obtained AC/CNT nanocomposites were still in powder form, and a binder was still needed.

Recently it has been shown that vertically aligned CNTs, in which the CNTs with large aspect ratio are well oriented, can be well dispersed into individually long CNTs by a two-step shearing strategy [45]. The as-obtained CNT pulp, in which long CNTs have good dispersion in the liquid phase, can be used as a feedstock for CNT transparent conductive films [45] and buckypaper [46]. As a result of great efforts to mass produce aligned CNTs, they can be easily produced by radial growth on spheres [47] or intercalated growth in lamellar catalysts [48]. A 3.0 kg/h productivity of aligned CNTs at a low cost has been achieved in a fluidized bed reactor [49]. This provides industrial grade aligned CNTs for practical applications in composites, catalysis, energy conversion and storage.

In this contribution, industrially produced aligned CNTs, together with AC powder, were used as raw materials to fabricate flexible electrodes. It is expected that the CNTs will bind AC particles together to give a paper-like composite. 90 wt%–99 wt% of AC was first incorporated into the CNT pulp, and the deposited on a filter to make composites. Flexible paper-like and binder-free electrodes with as high as 90 wt%–95 wt% of AC loading were obtained. The electrical conductivity, rate performance, and power density of the paper-like electrode were improved compared with the corresponding values for an AC/acetylene black (AB) electrode. The paper-like electrode also exhibited a good cycle performance.

2. Experimental

2.1 Aligned CNT production and purification

Aligned CNTs were mass-produced on a natural vermiculite catalyst in a fluidized bed reactor [50]. The CNTs in arrays had an inner diameter of 3–6 nm, an outer diameter of 7–12 nm, and a length of tens of micrometers. The vermiculite layers can be removed by impregnation in 3.0 mol/L HCl solution for 1.0 h followed by 1.0 mol/L HF solution. The CNT arrays still possessed good alignment after acid treatment [50].

2.2 AC/CNT paper electrode fabrication

Purified aligned CNTs were directly sheared in benzyl

alcohol [45]. About 210 mL of CNT suspension with a concentration of 100 mg/L was first stirred in a disintegrator for 30 min at a rotation speed of 6000 r/min. Then it was divided into five parts with the volumes of 10, 20, 30, 50, and 100 mL. Each of these was diluted to about 250 mL by benzyl alcohol and further stirred in the disintegrator for 30 min at a rotation speed of 6000 r/min. Then 0.1 g of AC was added to each suspension and the mixture stirred for 1 h at a rotation speed of 600 r/min. The as-obtained AC/CNT pulp was filtered through a nylon filter membrane (220 nm pore size) to remove benzyl alcohol. Another 100 mL of anhydrous ethyl alcohol was passed through the filter to remove benzyl alcohol. Finally, 100 mL of deionized water was passed through the filter to remove the ethyl alcohol. The filter cake was peeled off from the filter membrane and dried in an oven at 100 ℃ for 1 h. This process gave five AC/CNT paper electrodes with different CNT loadings. The as-obtained CNT paper electrodes are denoted AC-CNT-1%, AC-CNT-2%, AC-CNT-3%, AC-CNT-5%, and AC-CNT-10%. The AC/CNT paper electrodes were pressed against a piece of Ni foam directly under a pressure of 5.0 MPa. The area of the electrode for electrochemical tests was about 1.0 cm × 1.0 cm.

For the purposes of comparison, an AC/acetylene black (AB) electrode was also fabricated. AC, AB and PTFE were mixed in a mass ratio of 75:15:10 and dispersed in ethanol. Then the resulting mixture was coated onto the nickel foam substrate with a spatula, and dried at 100 ℃ for 6 h in an oven. The area of the electrode was also about 1.0 cm × 1.0 cm. The loading on each electrode was ca. 5.0 mg.

2.3 Characterization

Macroscopic photographs were taken using a Nikon 4500 digital camera. The microscopic morphology of the samples was characterized by scanning electron microscopy (SEM, JSM 7401F) operating at 3.0 kV. The electrical conductivity was measured by a four probe method. The AC/CNT paper-like composites with different CNT loadings were directly measured. AC, AB and PTFE were mixed in a mass ratio of 75:15:10 and dispersed in ethanol. The mixture was pressed between two pieces of paper and dried to make a disk-like material for conductivity tests. The N_2 adsorption and desorption isotherms were measured by N_2 adsorption at liquid N_2 temperature using a Micrometrics Flow Sorb Ⅱ 2300. The BET specific surface area was measured and the pore volume and pore size distribution was obtained using the Barrett–Joyner–Halenda (BJH) method.

The electrochemical measurements were conducted in a three-electrode setup: a Ni foam coated with electrode materials served as the working electrode, and a platinum foil electrode and a saturated calomel electrode (SCE) served as counter and reference electrodes, respectively. The measurements were carried out in a 6.0 mol/L KOH aqueous electrolyte at room temperature. Cyclic voltammograms (CV), galvanostatic charge/discharge, and electrochemical impedance spectroscopy (EIS) were measured using a Solartron 1470E electrochemical station equipped with a 1455A FRA module. CV tests were done between –1.0 and 0 V (vs. SCE) at different scan rates of 10, 20, 50, 100, and 200 mV/s. Galvanostatic charge/discharge curves were measured in the potential range –1.0 to 0 V (vs. SCE) at different current densities of 1, 2, 5, 10, and 20 A/g. EIS measurements were also carried out in the frequency range from 100 kHz to 0.1 Hz at open circuit potential with an ac perturbation of 5 mV. The Nyquist plots were fitted by Simpwin (ver. 3.10) software.

3. Results and discussion

It is difficult to handle AC powder as an electrode material for supercapacitors (Fig. 1(a)). Thus, a binder (such as PTFE) has to be added to maintain good mechanical properties. It has been demonstrated that aligned CNTs can be dispersed into long individual CNTs, and the as-obtained CNT pulp can be formed into CNT paper by filtration [46]. By adding the AC powder into CNT pulp, the CNTs bind AC particles together affording a flexible paper electrode. In order to utilize the high capacity of AC, the amount of AC should be as large as possible. Thus, 90 wt%–99 wt% of AC was first incorporated into CNT pulp. A typical macroscopic photograph of a flexible paper electrode with an AC loading as high as 95 wt% (AC-CNT-5%) is shown in Fig. 1(b). When the AC loading was between 90 wt%–95 wt%, the paper electrodes were highly

flexible and can be bent elastically (see the insert in Fig. 1(b)). The AC/CNT paper electrode can be expected to extend the applications of AC as an electrode material for supercapacitors.

An AC/AB electrode made of a mixture of AC with a traditional conductive agent, AB (15 wt%), and binder of PTFE (10 wt%) was used for comparison. SEM images of AC/AB and AC/CNT composite electrodes are shown in Fig. 2. The irregular AC particles had a size of about several tens of micrometers (Fig. 2(a)), while the AB existed as spherical particles with a diameter of 40–60 nm (see the insert in Fig. 2(b)). In the AC/AB electrode, the AB particles formed a conductive network surrounding the AC particles (Fig. 2(b)). With the addition of AB, the conductivity of the AC electrode was increased from 8.52×10^{-5} to 1.22×10^{-2} S/cm. However, the AC particles cannot be uniformly encapsulated by AB. Many AC particles are exposed at the surface of the electrode, which may reduce the performance of the AC electrode. For the AC/CNT composite with 99 wt% of AC (AC-CNT-1%), although a few large AC particles were exposed at the surface of the paper electrode (Fig. 2(c)), most of the small AC particles were well coated by the CNTs (see the high magnification SEM image in Fig. 2(d)). The 1 wt% of CNTs were well dispersed. The conductivity was increased to 0.83 S/cm (Fig. 3), four orders of magnitude higher than the conductivity of pristine AC (8.52×10^{-5} S/cm), indicating the formation of a conductive network. The conductivity was about two orders of magnitude higher than that of an AC/AB electrode containing 15 wt% of AB. When the CNT amount was increased to 5 wt% (AC-CNT-5%), most of the AC particles were well coated by CNTs (Figs. 2(e)–2(g)). The CNTs bind the AC particles together, and the mechanical strength of composites increased greatly and they could even be bent (Fig. 1(b)). The conductivity increased from 0.83 to 1.8 S/cm when the CNT amount increased from 1 wt% to 5 wt% (Fig. 3). According to the percolation theory, one-dimensional rod-like nanotubes are much more efficient in constructing percolation networks than the three-dimensional spherical AB particles [51, 52]. The dispersed CNTs from aligned CNTs used in this work were long CNTs (10–30 μm), rather than short ones (usually 0.5–2 μm) prepared from agglomerated CNTs. Thus, by adding 1 wt% of CNTs, the conductivity increased dramatically. The long CNTs also facilitated the fabrication of flexible AC/CNT

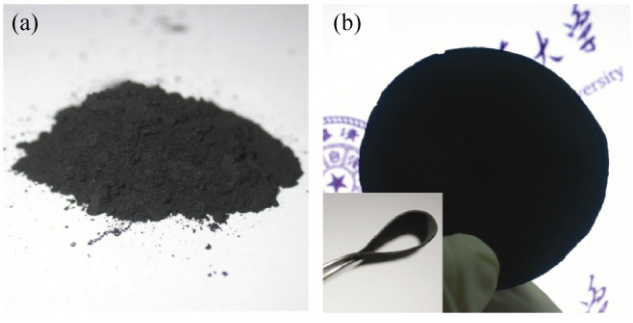

Figure 1 Macroscopic photographs of (a) AC powder and (b) AC-CNT-5% paper. The insert image shows the bending of the paper using a pair of tweezers

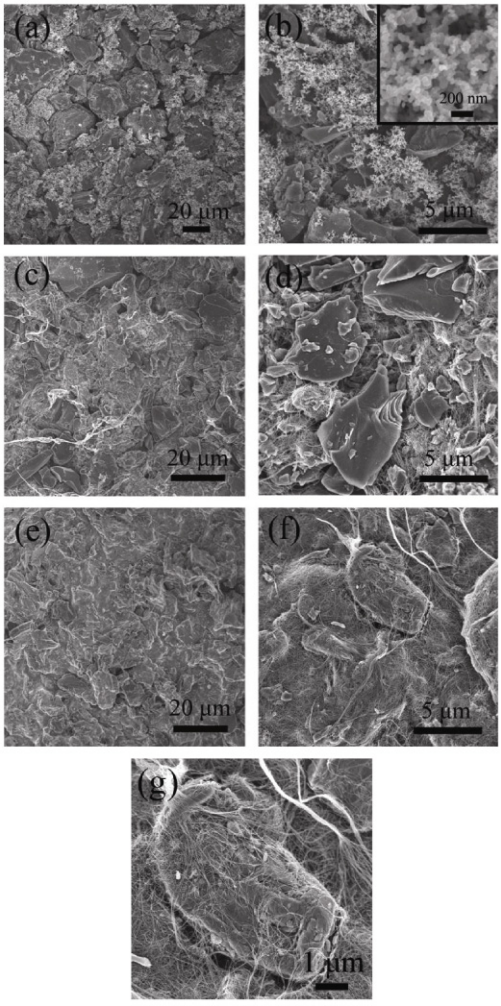

Figure 2 SEM images of (a), (b) an AC/AB electrode, (c), (d) an AC-CNT-1% electrode, and (e)–(g) an AC-CNT-5% electrode. The insert in (b) shows an enlarged image of the AB particles

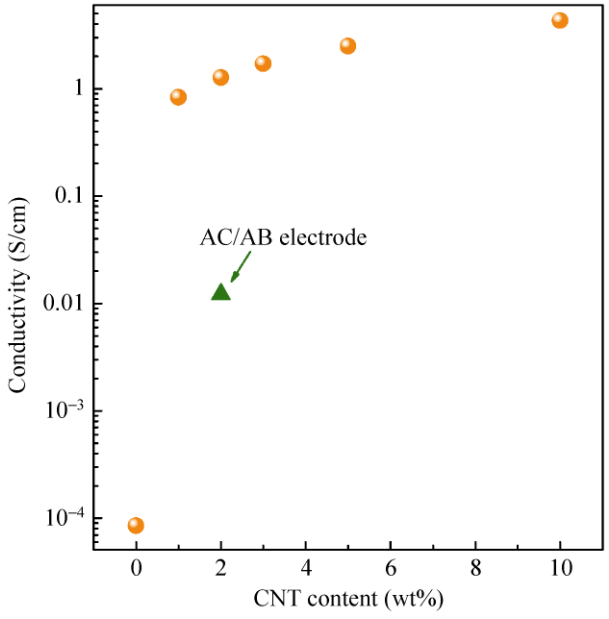

Figure 3 The conductivity of AC, AC/AB electrode (▲), and AC/CNT composite (●)

paper-like electrodes without the need to add an insulating binder such as PTFE, which also contributed to the enhanced conductivity compared with the AC/AB electrode. This will favor electron transport when used as an electrode for supercapacitors.

The specific surface area, pore volume and pore-size distribution are also the important factors affecting the electrochemical performance of supercapacitors. The N_2 adsorption isotherms and pore size distributions of AC powder, AC/AB and AC-CNT-5% electrodes and CNTs are shown in Figs. S-1(a)–S-1(c) in the Electronic Supplementary Material (ESM). The quantitative data extracted from the N_2 adsorption isotherms are given in Table S-1 (in the ESM). AC presents a type-I isotherm, which is typical for a microporous material. The BET surface area and average pore diameter of AC powder were 1374 m^2/g and 2.35 nm, respectively. After the addition of AB or CNTs, the N_2 adsorption was almost unmodified in the small relative pressure region corresponding to micropores, whereas a noticeable enhancement at $P/P_0 > 0.9$, in the range of mesoporosity, was observed.

The pore size distribution of CNTs showed two peaks at about 2.5 and 20 nm. The former may arise from the inner space of CNTs and the latter probably arise from the pores between CNTs [53, 54]. The pore size distribution of AC-CNT-5% also showed two small peaks at about 10 and 25 nm. The former may be generated by the pores in bundles of CNTs formed during the liquid phase process [53]. The latter results from the pores generated by the stacking of CNTs, and its size was slightly increased due to the presence of AC particles. The BET surface area and average pore diameter of AC/AB were 1011 m^2/g and 2.64 nm. The total pore volume decreased due to the addition of 15 wt% AB and 10 wt% PTFE. However, the ratio between the mesoporous and microporous volumes (V_{meso}/V_{micro}) was almost the same. The BET surface area and average pore diameter of AC-CNT-5% were 1223 m^2/g and 2.99 nm. The micropore volume of the AC was slightly diminished by the presence of CNTs, whereas the mesoporous volume increased from 0.32 to 0.38 cm^3/g. The V_{meso}/V_{micro} ratio showed a significant increase from 1.21 to 1.69. The enhanced mesoporous volume will favor the diffusion of ions during electrochemical processes [27, 55].

The CV curves of AC/AB and AC-CNT-5% electrodes at different scan rates are shown in Figs. 4(a) and 4(b). At a scan rate of 10 mV/s, the CV curve of the AC/AB electrode was close to a rectangular shape, without obvious redox peaks. However, when the scan rate was increased to 50 mV/s, the rectangle shape became severely distorted and it changed into a diamond shape when the scan rate was increased to 200 mV/s, indicative of a poor rate performance. The CV curve of AC-CNT-5% electrode was also close to a rectangular shape at a scan rate of 10 mV/s, indicating an ideal capacitive behavior. Even when the scan rate was increased to 200 mV/s, the shape of CV curve did not change dramatically, demonstrating an improved rate performance. Compared with the AC/AB electrode, the current at the AC-CNT paper electrode increased greatly, indicating an obvious improvement in the specific capacity.

The specific capacity of an electrode can be calculated according to the following equation:

$$C = \int \frac{I}{m} \mathrm{d}V \Big/ v\Delta V \quad (1)$$

where C is the specific capacity (F/g), I is the response current (A), m is the total mass of electrode materials

(g), ΔV is the potential range of CV (V), v is the potential scan rate (mV/s), and I/m is the current density (A/g).

The capacity of AC/CNT paper electrodes with different CNT loadings is shown in Fig. 4(c). As the CNT loading was increased from 2 wt% to 5 wt%, the capacity increased from 242.5 to 267.6 F/g. This can be attributed to the increase of electrical conductivity of the nanocomposite, which facilitates the electron transport during the CV scan process. However, it decreased to 233.4 F/g when the loading was increased to 10 wt%. Since the capacity of CNTs is only ca. 20 F/g [31, 56], the capacity can be mainly attributed to AC. Thus, the capacity decreased when the loading of CNTs was too high. The capacity reached a maximum value at a CNT loading of 5 wt%. It was also observed that the capacities of all the AC/CNT composites were higher than that of the AC/AB electrode (181.4 F/g), indicating that CNTs are better conductive agents than AB.

The relationships between capacity and scan rate for AC/AB and AC-CNT-5% electrodes are shown in Fig. 4(d). When the scan rate was increased, the capacity decreased. For the AC/AB electrode, the capacity was 199.7 F/g at a scan rate 10 mV/s. It decreased to 43.6 F/g at a scan rate of 200 mV/s, corresponding to only 21.8% of the value at 10 mV/s. However, for AC-CNT-5%, the capacity was 270.9 F/g at a scan rate 10 mV/s. It decreased to 160.5 F/g at the scan rate of 200 mV/s corresponding to 59.3% of the value at 10 mV/s, indicating a better rate performance (Fig. 4).

The galvanostatic charge/discharge curves of

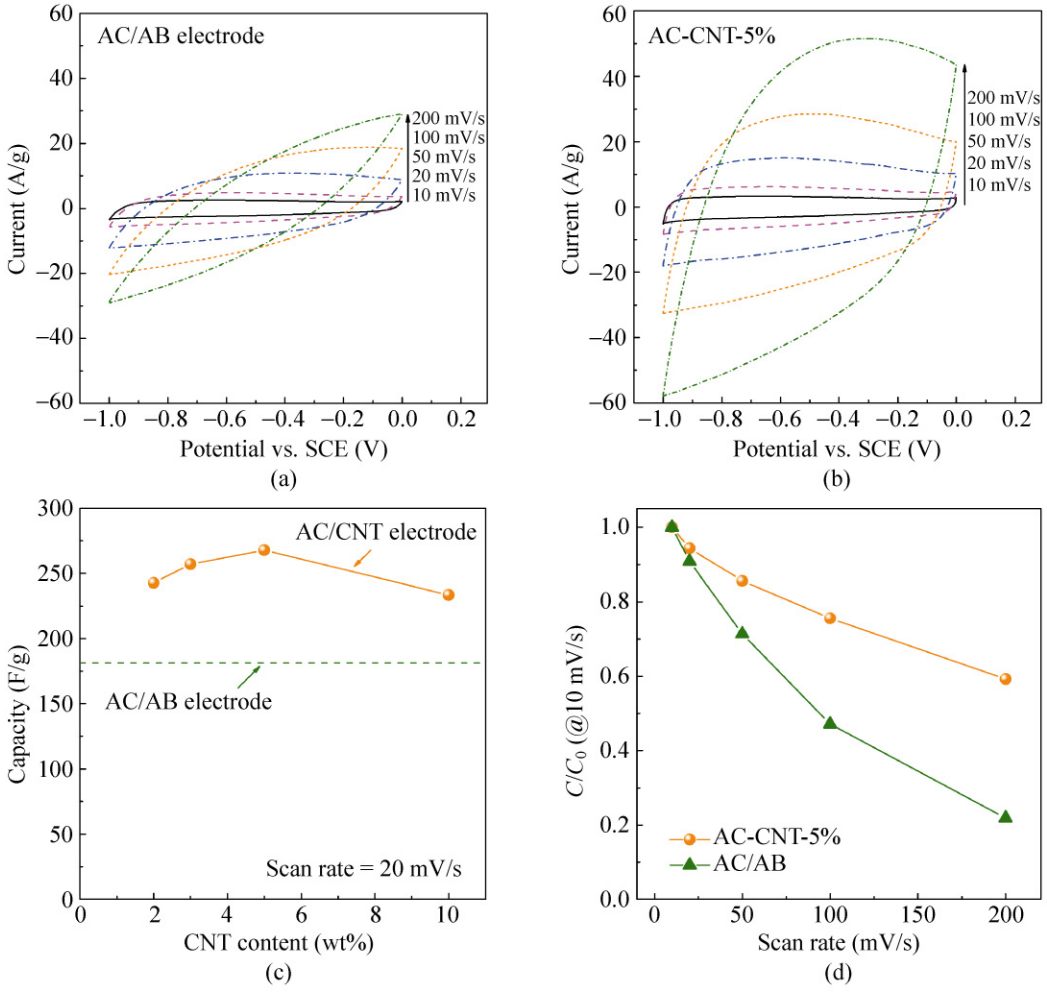

Figure 4 The CV curves of (a) AC/AB and (b) AC-CNT-5% electrodes at different scan rates. (c) The specific capacity of the AC/AB electrode and AC/CNT composites at a scan rate of 20 mV/s. (d) The relationship between capacity and scan rates for AC/AB and AC-CNT-5% electrodes

AC-CNT-5% at different current densities of 1, 2, 5, and 10 A/g are shown in Fig. 5(a). All the curves are linear and symmetrical, indicating that the paper electrode possessed excellent electrochemical reversibility and charge–discharge properties. The capacity can be calculated by dividing the electric quantity by the discharge time:

$$C = \frac{Q}{m\Delta V} = \frac{\int I\mathrm{d}t}{m\Delta V} = \frac{It_{\mathrm{discharge}}}{m(V - IR_{\mathrm{drop}})} = \frac{I}{m} \cdot \frac{t_{\mathrm{discharge}}}{V - IR_{\mathrm{drop}}} \quad (2)$$

where Q is the electric quantity during discharge, ΔV is the potential range of discharge (V), V is the potential at the end of charging (V), IR_{drop} is the initial potential change at the current reversal from charge to discharge (V), and $t_{\mathrm{discharge}}$ is the discharge time (s). When the current reversed from charge to discharge, an IR_{drop} occurred due to internal resistance. Thus, the effective potential range should be (V–IR_{drop}).

The capacities calculated from the discharge curve were 297.9, 282.6, 268.7, and 260.4 F/g at current densities of 1, 2, 5, and 10 A/g, respectively. When the current density was increased to 20 A/g, an obvious IR_{drop} of ca. 0.133 V was observed (Fig. 5(b)). For the AC/AB electrode, IR_{drop} was even as high as 0.485 V, some 3.6 times that of AC-CNT-5% electrode. The capacities were 256.0 and 190.1 F/g for AC-CNT-5% and AC/AB electrodes at a current density of 20 A/g, respectively. The AC-CNT-5% electrode had a higher energy density than that of AC/AB electrode. The relationship between IR_{drop} and current density of the two electrodes is plotted in Fig. 5(c), and both showed a linear behavior. The internal resistance of AC-CNT-5% electrode ($IR_{\mathrm{drop}}(V) = 0.0038 + 0.0065I$) was much lower

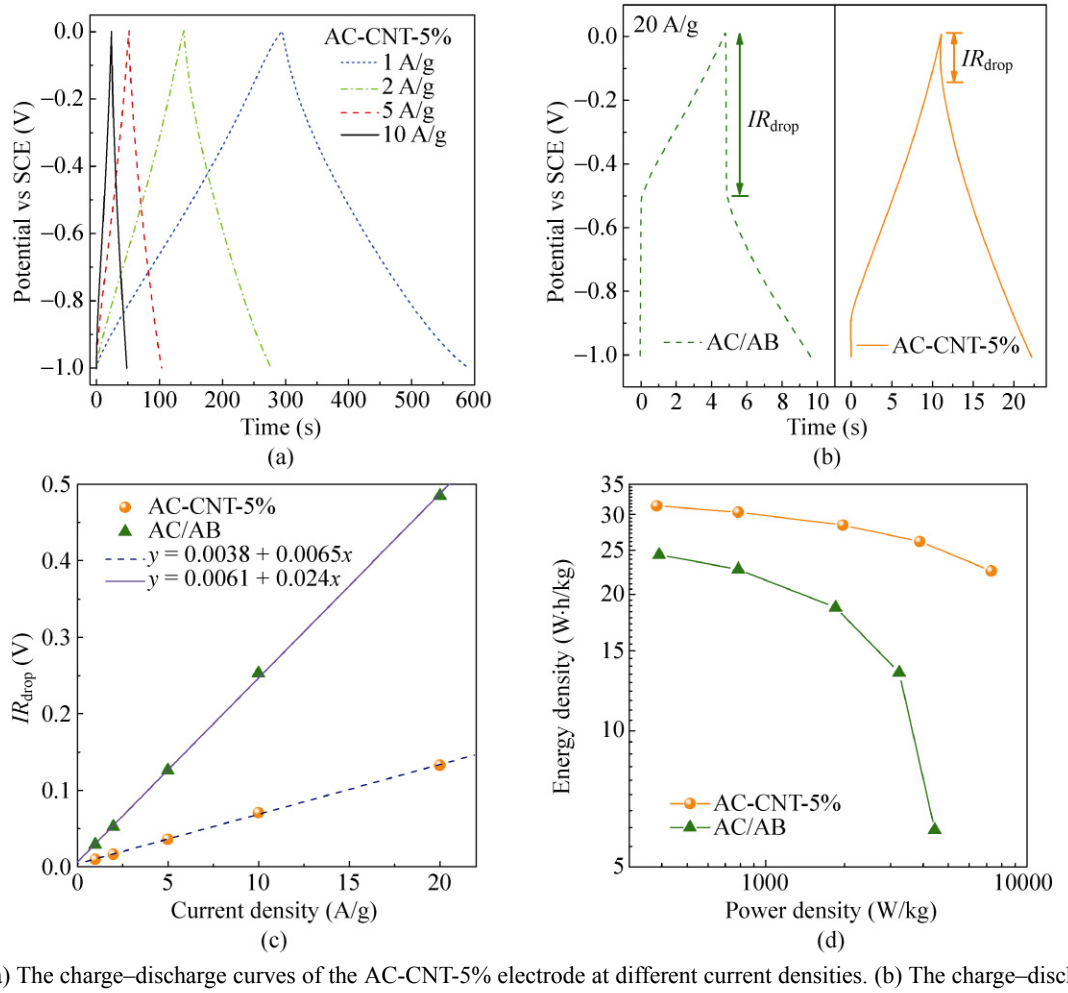

Figure 5 (a) The charge–discharge curves of the AC-CNT-5% electrode at different current densities. (b) The charge–discharge curves at 20 A/g. (c) The relationship between IR_{drop} and current density, and (d) the Ragone plots for AC/AB and AC-CNT-5% electrodes

than that of the AC/AB electrode ($IR_{drop}(V) = 0.0061 + 0.0024I$), indicating a better power density performance.

The energy density can be calculated by integrating the discharge curve, and the power density can be calculated by dividing the energy density by the discharge time. The equations are given below:

$$E = \frac{\int VI\mathrm{d}t}{m} = \frac{I}{m}\int V\mathrm{d}t \quad (3)$$

$$P = \frac{E}{t_{\mathrm{discharge}}} \quad (4)$$

where E is the energy density of the electrode material (W·h/kg), V is the potential vs. SCE (V), and P is the power density of the electrode material (W/kg). Ragone plots for AC/AB and AC-CNT-5% electrodes are shown in Fig. 5(d). Both the energy density and power density were improved for the AC-CNT-5% electrode, especially at a large current density of 20 A/g. The energy density and power density were 6.04 W·h/kg and 4.4 kW/kg for the AC/AB electrode, and 22.5 W·h/kg and 7.3 kW/kg for AC-CNT-5% paper electrode. Both the enhanced conductivity and mesoporous volume play important roles in the improvement of power density.

EIS analysis is one of the principal methods examining the fundamental behavior of electrode materials for supercapacitors. The Nyquist plots for AC/AB and AC-CNT-5% are shown in Fig. 6. From the enlarged view in Fig. 6(b), the internal resistances (i.e., the intercept at the *Re* (*Z*) axis) were 0.33 Ω (12.6 kHz) and 0.46 Ω (10 kHz) for AC-CNT-5% and AC/AB electrodes, respectively. Because the capacitive response was fast for these electrodes, their internal resistances were obtained at frequencies larger than 1 kHz. The standard equivalent series resistances (ESR) measured at 1 kHz were also obtained for comparison: 0.46 Ω for the AC-CNT-5% electrode and 0.52 Ω for the AC/AB electrode. The values of the internal resistance and ESR indicated that the addition of CNTs decreased the resistance, which was in good accordance with the conductivity test shown in Fig. 3. Furthermore, the impedance curve intersected the real axis ($Re(Z)$) at a 45° angle, is consistent with the porous nature of the electrode when saturated with electrolyte [57]. Usually, the knee frequency represents not only the maximum frequency where the capacitive behavior is dominant, but also the power capability of a supercapacitor [15, 58]. The knee frequency of the AC-CNT-5% electrode was 31.6 Hz, higher than the value of 25.1 Hz for the AC/AB electrode, indicating better power capability. The results are in agreement with the power density data in Fig. 5(d).

The insert in Fig. 6(a) shows an equivalent circuit model to simulate the capacitive and resistive elements of the cells under analysis. These elements include the internal resistance (R_i), the capacitance and resistance

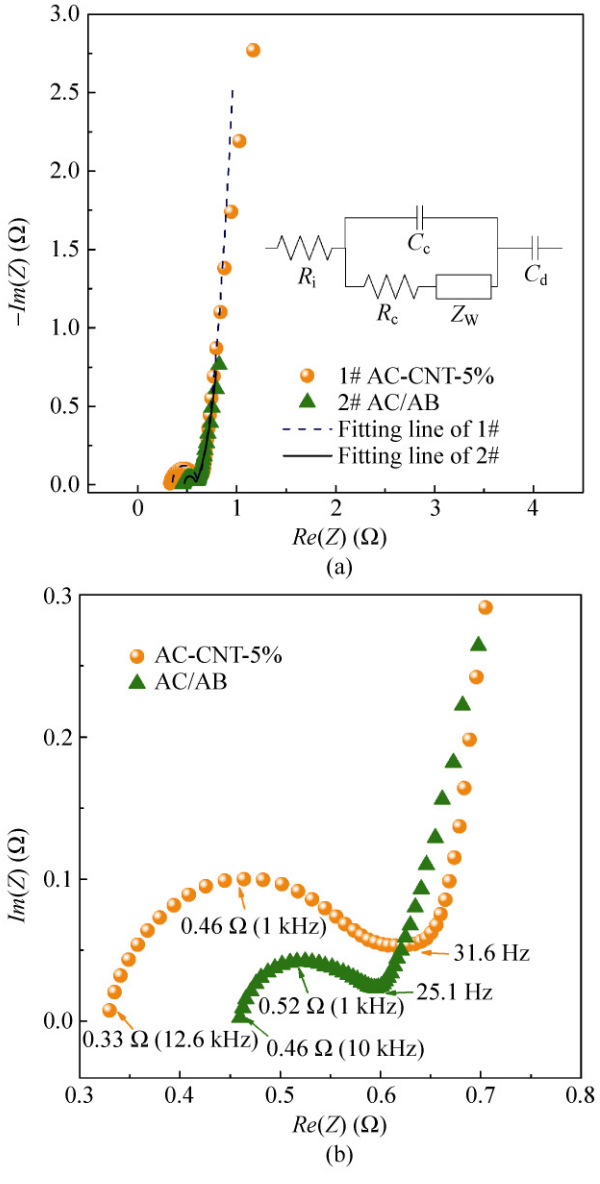

Figure 6 Nyquist plots of AC/AB and AC-CNT-5% electrodes and the fitting curves. The insert in (a) is the equivalent circuit. (b) is an enlarged view of (a)

due to the contact interface (C_c and R_c), a Warburg diffusion element attributable to the ion migration through the carbon film (Z_W), and the capacitance inside the pores, C_d [59, 60]. The Warburg element is given by

$$Z_W = \frac{W}{\sqrt{j\omega}} \quad (5)$$

$$W = \frac{RT}{n^2F^2Ac\sqrt{D_e}} \quad (6)$$

where j is the imaginary unit ($j = \sqrt{-1}$), ω is the angular frequency, W is the Warburg parameter in units of $\Omega/s^{1/2}$, R is the gas constant, T is the absolute temperature, n is the number of electrons transferred, F is the Faraday constant, A is the geometric electrode area, c is the electrolyte concentration, and D_e is the effective diffusivity for electrolyte motion in carbon electrodes. This shows that the Warburg parameter is a decreasing function of ionic conductivity. The impedance data in Fig. 6(a) were fitted to this model, and the fitting parameters are shown in Table 1. Ionic transportation was promoted for the AC-CNT-5% electrode ($W = 2.41\ \Omega/s^{1/2}$) compared with the AC/AB electrode ($W = 4.09\ \Omega/s^{1/2}$). However, the R_c for the AC-CNT-5% electrode (0.24 Ω) was higher than that of the AC/AB electrode (0.10 Ω). Since the CNTs were directly used without functionalization, the contact resistance with aqueous solution was high. The C_d increased, which is in agreement with the capacity data in Fig. 4(c).

Table 1 Fitting parameters of the Nyquist plots for AC/AB and AC-CNT-5% electrodes

Sample	R_i (Ω)	R_c (Ω)	C_c (F/g)	W ($\Omega/s^{1/2}$)	C_d (F/g)
AC/AB	0.47	0.10	0.1	4.09	132
AC-CNT-5%	0.35	0.24	0.14	2.41	158

The cycle stability of supercapacitors is a crucial parameter for practical applications. The cycle stability of the AC-CNT-5% electrode was evaluated by repeating the CV test between –1.0 and 0 V (vs. SCE) at a scan rate of 200 mV/s for 5000 cycles. The capacitance retention ratio as a function of cycle number is presented in Fig. 7. The capacitance only decreased by 2.5% of the initial capacitance after 5000 cycles, and the shapes of the CV curves before and after 5000 cycles were almost the same (Fig. 7, insert), demonstrating the excellent electrochemical stability of the flexible paper nanocomposite electrode.

There have been previous reports of the combination of carbon materials with conductive polymers or metal oxides to obtain flexible CNT/PANI [36, 37], CNF/PANI [10], graphene/PANI or graphene oxide/PANI [14, 16, 38], or CNT/CuO [39] composite electrodes with improved electrochemical performance. In these materials, a thin PANI layer (several tens to hundreds of nanometers) was usually coated onto the surface of CNT, CNF or graphene materials to obtain flexible composites [10, 14, 16, 36–38]. Nanoparticles, nanowires or nanobelts of metal oxide have also been combined with CNTs to obtain flexible composites [39, 40]. Such nanoarchitecture gives rise to an increase the contact surface area between the electrode, and a decrease in the transport path length for both electrons and ions [31]. We have demonstrated the feasibility of fabricating flexible composites using AC particles several tens of micrometers in size. Furthermore, the method can also be employed to fabricate flexible composites with nanostructured conductive polymer or metal oxides in order to meet the needs of versatile applications in devices such as flexible lithium ion batteries and solar cells.

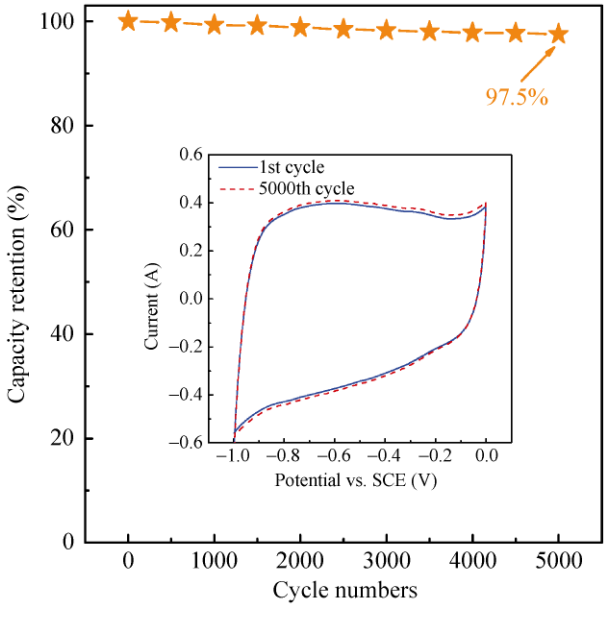

Figure 7 The cycle performance of AC-CNT-5% at a scan rate of 200 mV/s. The insert shows the CV curves of the 1st and 5000th cycles

4. Conclusions

Aligned CNTs, which can be mass produced in a fluidized bed reactor at an industrial scale at a low cost, were first sheared to obtain CNT pulp. Then 90 wt%–99 wt% of AC powder was incorporated into the CNT pulp and passed through a filter to make a composite. Flexible and binder-free paper-like AC/CNT electrodes with 90 wt%–95 wt% AC loading were obtained. Due to the availability of long CNTs, a more effective conductive network was formed. The mesoporous volume was also enhanced due to the addition of CNTs. The capacity reached a maximum value of 267.6 F/g (at a scan rate of 200 mV/s) at a CNT loading of 5 wt%. The rate performance was improved and the capacitance retention ratio increased from 21.8% for the AC/AB electrode to 59.3% for the AC-CNT-5% electrode, when the scan rate changed from 10 to 200 mV/s. The internal resistance of the AC-CNT-5% electrode ($IR_{drop}(V) = 0.0038 + 0.0065I$) was much lower than that of the AC/AB electrode ($IR_{drop}(V) = 0.0061 + 0.0024I$). The energy density and power density were 22.5 W·h/kg and 7.3 kW/kg for the AC-CNT-5% electrode, and 6.04 W·h/kg and 4.4 kW/kg for the AC/AB electrode at a large current density of 20 A/g. The internal resistance and ESR decreased and the knee frequency increased for AC-CNT-5%. By fitting the EIS spectra, the Warburg parameter also decreased, indicating better ionic conductivity. The AC-CNT-5% electrode also showed a good cycle performance, with the capacity retaining 97.5% of the original value after 5000 cycles at a scan rate of 200 mV/s. These properties show this paper nanocomposite is a promising material for use in low-cost and flexible supercapacitors. Furthermore, the method can also be employed to fabricate various kinds of CNT-based composite papers with different properties in order to meet the requirements for applications in devices such as flexible lithium ion batteries and solar cells.

Acknowledgements

This study was supported by the National Natural Science Foundation of China (Nos. 20736004, 20736007, and 2007AA03Z346), and the China National Program (No. 2011CB932602).

Electronic Supplementary Material: Supplementary material (N_2 adsorption isotherms at 77 K, pore size distribution and physicochemical characteristics of AC powder, AC/AB and AC-CNT-5% electrodes and CNTs) is available in the online version of this article at http://dx.doi.org/ 10.1007/s12274-011-0143-8.

References

[1] Rogers, J. A. Toward paperlike displays. *Science* **2001**, *291*, 1502–1503.

[2] Rogers, J. A.; Someya, T.; Huang, Y. G. Materials and mechanics for stretchable electronics. *Science* **2010**, *327*, 1603–1607.

[3] Kaempgen, M.; Chan, C. K.; Ma, J.; Cui, Y.; Gruner, G. Printable thin film supercapacitors using single-walled carbon nanotubes. *Nano Lett.* **2009**, *9*, 1872–1876.

[4] Hu, L. B.; Pasta, M.; La Mantia, F.; Cui, L. F.; Jeong, S.; Deshazer, H. D.; Choi, J. W.; Han, S. M.; Cui, Y. Stretchable, porous, and conductive energy textiles. *Nano Lett.* **2010**, *10*, 708–714.

[5] Nishide, H.; Oyaizu, K. Toward flexible batteries. *Science* **2008**, *319*, 737–738.

[6] Li, X.; Rong, J. P.; Wei, B. Q. Electrochemical behavior of single-walled carbon nanotube supercapacitors under compressive stress. *ACS Nano* **2010**, *4*, 6039–6049.

[7] Bae, J.; Song, M. K.; Park, Y. J.; Kim, J. M.; Liu, M. L.; Wang, Z. L. Fiber supercapacitors made of nanowire-fiber hybrid structures for wearable/flexible energy storage. *Angew. Chem. Int. Ed.* **2011**, *50*, 1683–1687.

[8] Chen, Y. S.; Xu, Y. F.; Zhao, K.; Wan, X. J.; Deng, J. C.; Yan, W. B. Towards flexible all-carbon electronics: Flexible organic field-effect transistors and inverter circuits using solution-processed all-graphene source/drain/gate electrodes. *Nano Res.* **2010**, *3*, 714–721.

[9] Chen, C. M.; Yang, Q. H.; Yang, Y. G.; Lv, W.; Wen, Y. F.; Hou, P. X.; Wang, M. Z.; Cheng, H. M. Self-assembled free-standing graphite oxide membrane. *Adv. Mater.* **2009**, *21*, 3007–3011.

[10] Yan, X. B.; Tai, Z. X.; Chen, J. T.; Xue, Q. J. Fabrication of carbon nanofiber–polyaniline composite flexible paper for supercapacitor. *Nanoscale* **2011**, *3*, 212–216.

[11] Nyholm, L.; Nyström, G.; Mihranyan, A.; Strømme, M. Toward flexible polymer and paper-based energy storage devices. *Adv. Mater.* **2011**, DOI: 10.1002/adma.201004134.

[10] Snook, G. A.; Kao, P.; Best, A. S. Conducting-polymer-based supercapacitor devices and electrodes. *J. Power Sources* **2011**, *196*, 1–12.

[13] Li, G. R.; Feng, Z. P.; Ou, Y. N.; Wu, D. C.; Fu, R. W.; Tong,

Y. X. Mesoporous MnO_2/carbon aerogel composites as promising electrode materials for high-performance supercapacitors. *Langmuir* **2010**, *26*, 2209–2213.

[14] Yan, J.; Wei, T.; Shao, B.; Fan, Z. J.; Qian, W. Z.; Zhang, M. L.; Wei, F. Preparation of a graphene nanosheet/polyaniline composite with high specific capacitance. *Carbon* **2010**, *48*, 487–493.

[15] Chen, P. C.; Chen, H. T.; Qiu, J.; Zhou, C. W. Inkjet printing of single-walled carbon nanotube/RuO_2 nanowire supercapacitors on cloth fabrics and flexible substrates. *Nano Res.* **2010**, *3*, 594–603.

[16] Wang, D. W.; Li, F.; Zhao, J. P.; Ren, W. C.; Chen, Z. G.; Tan, J.; Wu, Z. S.; Gentle, I.; Lu, G. Q.; Cheng, H. M. Fabrication of graphene/polyaniline composite paper via in situ anodic electropolymerization for high-performance flexible electrode. *ACS Nano* **2009**, *3*, 1745–1752.

[17] Kang, Y. J.; Kim, B.; Chung, H.; Kim, W. Fabrication and characterization of flexible and high capacitance supercapacitors based on MnO_2/CNT/papers. *Synth. Met.* **2011**, *160*, 2510–2514.

[18] Izadi-Najafabadi, A.; Yasuda, S.; Kobashi, K.; Yamada, T.; Futaba, D. N.; Hatori, H.; Yumura, M.; Iijima, S.; Hata, K. Extracting the full potential of single-walled carbon nanotubes as durable supercapacitor electrodes operable at 4 V with high power and energy density. *Adv. Mater.* **2010**, *22*, E235–E241.

[19] Niu, Z. Q.; Zhou, W. Y.; Chen, J.; Feng, G. X.; Li, H.; Ma, W. J.; Li, J. Z.; Dong, H. B.; Ren, Y.; Zhao, D.; Xie, S. S. Compact-designed supercapacitors using free-standing single-walled carbon nanotube films. *Energy Environ. Sci.* **2011**, *4*, 1440–1446.

[20] Zhang, L. L.; Zhao, X. S. Carbon-based materials as supercapacitor electrodes. *Chem. Soc. Rev.* **2009**, *38*, 2520–2531.

[21] Frackowiak, E.; Beguin, F. Carbon materials for the electrochemical storage of energy in capacitors. *Carbon* **2001**, *39*, 937–950.

[22] Liu, C. G.; Yu, Z. N.; Neff, D.; Zhamu, A.; Jang, B. Z. Graphene-based supercapacitor with an ultrahigh energy density. *Nano Lett.* **2010**, *10*, 4863–4868.

[23] Zhang, L. L.; Zhou, R.; Zhao, X. S. Graphene-based materials as supercapacitor electrodes. *J. Mater. Chem.* **2010**, *20*, 5983–5992.

[24] Zhao, X. C.; Wang, A. Q.; Yan, J. W.; Sun, G. Q.; Sun, L. X.; Zhang, T. Synthesis and electrochemical performance of heteroatom-incorporated ordered mesoporous carbons. *Chem. Mater.* **2010**, *22*, 5463–5473.

[25] Yang, X. Q.; Wu, D. C.; Chen, X. M.; Fu, R. W. Nitrogen-enriched nanocarbons with a 3-D continuous mesopore structure from polyacrylonitrile for supercapacitor application. *J. Phys. Chem. C* **2010**, *114*, 8581–8586.

[26] Wu, D. C.; Chen, X.; Lu, S. H.; Liang, Y. R.; Xu, F.; Fu, R. W. Study on synergistic effect of ordered mesoporous carbon and carbon aerogel during electrochemical charge-discharge process. *Micropor. Mesopor. Mater.* **2010**, *131*, 261–264.

[27] Wang, D. W.; Li, F.; Liu, M.; Lu, G. Q.; Cheng, H. M. 3D aperiodic hierarchical porous graphitic carbon material for high-rate electrochemical capacitive energy storage. *Angew. Chem. Int. Ed.* **2008**, *47*, 373–376.

[28] Chmiola, J.; Largeot, C.; Taberna, P. L.; Simon, P.; Gogotsi, Y. Monolithic carbide-derived carbon films for micro-supercapacitors. *Science* **2010**, *328*, 480–483.

[29] Fan, Z. J.; Yan, J.; Zhi, L. J.; Zhang, Q.; Wei, T.; Feng, J.; Zhang, M. L.; Qian, W. Z.; Wei, F. A three-dimensional carbon nanotube/graphene sandwich and its application as electrode in supercapacitors. *Adv. Mater.* **2010**, *22*, 3723–3728.

[30] Beguin, F.; Szostak, K.; Lota, G.; Frackowiak, E. A self-supporting electrode for supercapacitors prepared by one-step pyrolysis of carbon nanotube/polyacrylonitrile blends. *Adv. Mater.* **2005**, *17*, 2380–2384.

[31] Su, D. S.; Schlogl, R. Nanostructured carbon and carbon nanocomposites for electrochemical energy storage applications. *ChemSusChem* **2010**, *3*, 136–168.

[32] Yuan, C. Z.; Gao, B.; Shen, L. F.; Yang, S. D.; Hao, L.; Lu, X. J.; Zhang, F.; Zhang, L. J.; Zhang, X. G. Hierarchically structured carbon-based composites: Design, synthesis and their application in electrochemical capacitors. *Nanoscale* **2011**, *3*, 529–545.

[33] Zhang, H.; Cao, G. P.; Wang, Z. Y.; Yang, Y. S.; Shi, Z. J.; Gu, Z. N. Growth of manganese oxide nanoflowers on vertically-aligned carbon nanotube arrays for high-rate electrochemical capacitive energy storage. *Nano Lett.* **2008**, *8*, 2664–2668.

[34] Zhang, H.; Cao, G. P.; Wang, W. K.; Yuan, K. G.; Xu, B.; Zhang, W. F.; Cheng, J.; Yang, Y. S. Influence of microstructure on the capacitive performance of polyaniline/carbon nanotube array composite electrodes. *Electrochim. Acta* **2009**, *54*, 1153–1159.

[35] Yan, J.; Fan, Z. J.; Wei, T.; Qian, W. Z.; Zhang, M. L.; Wei, F. Fast and reversible surface redox reaction of graphene–MnO_2 composites as supercapacitor electrodes. *Carbon* **2010**, *48*, 3825–3833.

[36] Meng, C. Z.; Liu, C. H.; Chen, L. Z.; Hu, C. H.; Fan, S. S. Highly flexible and all-solid-state paper like polymer supercapacitors. *Nano Lett.* **2010**, *10*, 4025–4031.

[37] Meng, C. Z.; Liu, C. H.; Fan, S. S. Flexible carbon nanotube/polyaniline paper-like films and their enhanced electrochemical properties. *Electrochem. Commun.* **2009**, *11*, 186–189.

[38] Yan, X. B.; Chen, J. T.; Yang, J.; Xue, Q. J.; Miele, P. Fabrication of free-standing, electrochemically active, and biocompatible graphene oxide–polyaniline and graphene–polyaniline hybrid papers. *ACS Appl. Mater. Interf.* **2010**, *2*, 2521–2529.

[39] Zhang, X. J.; Shi, W. H.; Zhu, J. X.; Kharistal, D. J.; Zhao, W. Y.; Lalia, B. S.; Hng, H. H.; Yan, Q. Y. High-power and high-energy-density flexible pseudocapacitor electrodes made from porous CuO nanobelts and single-walled carbon nanotubes. *ACS Nano* **2011**, *5*, 2013–2019.

[40] Lima, M. D.; Fang, S. L.; Lepro, X.; Lewis, C.; Ovalle-Robles, R.; Carretero-Gonzalez, J.; Castillo-Martinez, E.; Kozlov, M. E.; Oh, J. Y.; Rawat, N., Haines, C. S.; Haque, M. H.; Are, V.; Stoughton, S.; Zakhidov, A. A.; Baughman, R. H. Biscrolling nanotube sheets and functional guests into yarns. *Science* **2011**, *331*, 51–55.

[41] Pico, F.; Pecharroman, C.; Anson, A.; Martinez, M. T.; Rojo, J. M. Understanding carbon–carbon composites as electrodes of supercapacitors—A study by AC and DC measurements. *J. Electrochem. Soc.* **2007**, *154*, A579–A586.

[42] Taberna, P. L.; Chevallier, G.; Simon, P.; Plee, D.; Aubert, T. Activated carbon–carbon nanotube composite porous film for supercapacitor applications. *Mater. Res. Bull.* **2006**, *41*, 478–484.

[43] Raymundo-Piñero, E.; Cadek, M.; Wachtler, M.; Béguin, F. Carbon nanotubes as nanotexturing agents for high power supercapacitors based on seaweed carbons. *ChemSusChem* DOI:10.1002/cssc.201000376.

[44] Portet, C.; Taberna, P. L.; Simon, P.; Flahaut, E. Influence of carbon nanotubes addition on carbon–carbon supercapacitor performances in organic electrolyte. *J. Power Sources* **2005**, *139*, 371–378.

[45] Xu, G. H.; Zhang, Q.; Huang, J. Q.; Zhao, M. Q.; Zhou, W. P.; Wei, F. A two-step shearing strategy to disperse long carbon nanotubes from vertically aligned multiwalled carbon nanotube arrays for transparent conductive films. *Langmuir* **2010**, *26*, 2798–2804.

[46] Xu, G. H.; Zhang, Q.; Zhou, W. P.; Huang, J. Q.; Wei, F. The feasibility of producing MWCNT paper and strong MWCNT film from VACNT array. *Appl. Phys. A* **2008**, *92*, 531–539.

[47] Zhang, Q.; Huang, J. Q.; Zhao, M. Q.; Qian, W. Z.; Wang, Y.; Wei, F. Radial growth of vertically aligned carbon nanotube arrays from ethylene on ceramic spheres. *Carbon* **2008**, *46*, 1152–1158.

[48] Zhang, Q.; Zhao, M. Q.; Liu, Y.; Cao, A. Y.; Qian, W. Z.; Lu, Y. F.; Wei, F. Energy-absorbing hybrid composites based on alternate carbon-nanotube and inorganic layers. *Adv. Mater.* **2009**, *21*, 2876–2880.

[49] Zhang, Q.; Zhao, M. Q.; Huang, J. Q.; Nie, J. Q.; Wei, F. Mass production of aligned carbon nanotube arrays by fluidized bed catalytic chemical vapor deposition. *Carbon* **2010**, *48*, 1196–1209.

[50] Zhang, Q.; Zhao, M. Q.; Huang, J. Q.; Liu, Y.; Wang, Y.; Qian, W. Z.; Wei, F. Vertically aligned carbon nanotube arrays grown on a lamellar catalyst by fluidized bed catalytic chemical vapor deposition. *Carbon* **2009**, *47*, 2600–2610.

[51] Bauhofer, W.; Kovacs, J. Z. A review and analysis of electrical percolation in carbon nanotube polymer composites. *Compos. Sci. Technol.* **2009**, *69*, 1486–1498.

[52] Bose, S.; Khare, R. A.; Moldenaers, P. Assessing the strengths and weaknesses of various types of pre-treatments of carbon nanotubes on the properties of polymer/carbon nanotubes composites: A critical review. *Polymer* **2010**, *51*, 975–993.

[53] Whitby, R. L. D.; Fukuda, T.; Maekawa, T.; James, S. L.; Mikhalovsky, S. V. Geometric control and tuneable pore size distribution of buckypaper and buckydiscs. *Carbon* **2008**, *46*, 949–956.

[54] Zhao, M. Q.; Zhang, Q.; Huang, J. Q.; Nie, J. Q.; Wei, F. Advanced materials from natural materials: Synthesis of aligned carbon nanotubes on wollastonites. *ChemSusChem* **2010**, *3*, 453–459.

[55] Xu, F.; Cai, R. J.; Zeng, Q. C.; Zou, C.; Wu, D. C.; Li, F.; Lu, X. E.; Liang, Y. R.; Fu, R. W. Fast ion transport and high capacitance of polystyrene-based hierarchical porous carbon electrode material for supercapacitors. *J. Mater. Chem.* **2011**, *121*, 1970–1976.

[56] Futaba, D. N.; Hata, K.; Yamada, T.; Hiraoka, T.; Hayamizu, Y.; Kakudate, Y.; Tanaike, O.; Hatori, H.; Yumura, M.; Iijima, S. Shape-engineerable and highly densely packed single-walled carbon nanotubes and their application as super-capacitor electrodes. *Nat. Mater.* **2006**, *5*, 987–994.

[57] Niu, C. M.; Sichel, E. K.; Hoch, R.; Moy, D.; Tennent, H. High power electrochemical capacitors based on carbon nanotube electrodes. *Appl. Phys. Lett.* **1997**, *70*, 1480–1482.

[58] Du, C. S.; Pan, N. High power density supercapacitor electrodes of carbon nanotube films by electrophoretic deposition. *Nanotechnology* **2006**, *17*, 5314–5318.

[59] Huang, C. W.; Hsu, C. H.; Kuo, P. L.; Hsieh, C. T.; Teng, H. S. Mesoporous carbon spheres grafted with carbon nanofibers for high-rate electric double layer capacitors. *Carbon* **2011**, *49*, 895–903.

[60] Huang, C. W.; Chuang, C. M.; Ting, J. M.; Teng, H. S. Significantly enhanced charge conduction in electric double layer capacitors using carbon nanotube-grafted activated carbon electrodes. *J. Power Sources* **2008**, *183*, 406–410.